AIAA JOURNAL
Vol. 35, No. 2, February 1997

Near-Wall Reynolds-Stress Three-Dimensional Transonic Flow Computation

G. A. Gerolymos* and I. Vallet†
Université Pierre-et-Marie-Curie, Orsay, Paris 91405, France

A computational method for the Favre–Reynolds-averaged three-dimensional compressible Navier–Stokes equations using near-wall Reynolds-stress closure is described. The near-wall Reynolds-stress closure uses the Launder–Shima (Launder, B. E., and Shima, N., "2-Moment Closure for the Near-Wall Sublayer: Development and Application," *AIAA Journal*, Vol. 27, No. 10, 1989, pp. 1319–1325) formulation for the Reynolds stresses and the Jones–Launder–Sharma modified dissipation (ε^*) equation (Launder, B. E., and Sharma, B. I., "Application of the Energy Dissipation Model of Turbulence to the Calculation of Flows near a Spinning Disk," *Letters in Heat and Mass Transfer*, Vol. 1, 1974, pp. 131–138). The mean-flow and turbulence-transport equations are discretized using a finite volume method based on MUSCL Van Leer flux–vector-splitting with Van Albada limiters. The mean-flow and turbulence equations are integrated in time using a fully coupled approximately factored implicit backward Euler method. The resulting scheme is robust and achieves optimal convergence with local-time-step Courant–Friedrichs–Lewy = 50. The turbulence closure is validated by comparison with classic flat-plate boundary-layer data. Results are presented for the three-dimensional Délery transonic channel test case and compared with *k*–ε computations. An analysis of the limitations of the closure is attempted, and possible improvements are suggested.

Introduction

REYNOLDS-STRESS closures in complex turbulent flows are usually coupled with wall functions.[1,2] Modeling work of the near-wall low-turbulence Reynolds-number effects has been based mostly on simple channel or boundary-layer flows.[3–6] There are very few successful efforts to incorporate near-wall Reynolds-stress closures in computational methods for complex flows. Sotiropoulos and Patel[7,8] used the Launder–Shima[9] model with the modification of the dissipation equation reported by Shima[10,11] to compute incompressible three-dimensional flow in a duct of varying cross section with strong secondary flows, and complex three-dimensional ship stern and wake flows. Recently, Ladeinde[12] developed and applied a compressible near-wall Reynolds-stress closure to the computation of two-dimensional supersonic boundary layers and two-dimensional shock-wave/boundary-layer interaction over a ramp.

The purpose of this work is to use a near-wall Reynolds stress model (RSM) for the computation of three-dimensional shock-wave/boundary-layer interaction, with strong detachment, in a transonic channel. Initially the Launder–Shima[9] model was used, but the ψ_1 and ψ_2 terms in the dissipation equation induced nonphysical relaminarization in the supersonic acceleration region. Problems with the ψ_1 and ψ_2 terms in the dissipation equation already have been noted by Shima[10,11] and Sotiropoulos and Patel.[7] An attempt to use the Launder–Shima model[9] without the ψ_1 and ψ_2 terms was successful for simple boundary-layer flows, but catastrophically unstable for shock-wave/boundary-layer interaction. The instability was associated with the use of the nonmodified dissipation equation, and particularly with the wall boundary condition $\varepsilon_w = 2\nu_w(\partial\sqrt{k}/\partial n)^2$. This instability is encountered near the wall in the initial phase of the computations. For the k–$\varepsilon*$ equations, the problem is easily solved because the homogeneous boundary condition for the modified dissipation $\varepsilon^*_w = 0$ is much stabler and more compatible with the simple limiters used.[13] To obtain a robust method, it was decided to use a hybrid model, built with the Launder–Shima[9] Reynolds-stress equations and the Jones–Launder–Sharma[14–16] modified dissipation equation.

This choice may at first appear unwise because the dissipation equation often has been fingered as the culprit of turbulence model deficiencies. Nonetheless, any nonmodified dissipation closure can be transformed to a modified dissipation equation after some manipulation. The numerical stability enhancement is worth the trouble.

The hybrid model used in this work was validated with respect to the classic flat-plate boundary-layer data of Klebanoff,[17] and evaluated against experimental measurements for a three-dimensional shock-wave/boundary-layer interaction.[18,19] Possible improvements of the model are discussed.

Flow Model

Reynolds-Stress Transport

Denoting t the time, x_l the Cartesian space coordinates, u_i the velocity components, ρ the density, p the pressure, $D_{ij} = \frac{1}{2}(\partial u_i/\partial x_j + \partial u_j/\partial x_i)$ the rate-of-deformation tensor of which the trace is the dilatation $\Theta = D_{ll} = \partial u_l/\partial x_l$, δ_{ij} the Kronecker symbol, $\tau_{ij} = \mu(2D_{ij} - \frac{2}{3}\Theta\delta_{ij})$ the viscous stresses, C_{ij} the convection of $\widetilde{u_i''u_j''}$, d_{ij} the diffusion due to viscous and turbulent transport T_{ijk}, ϕ_{ij} the redistribution tensor ($\phi_{ii} = 0$), P_{ij} the production due to mean-flow gradients, ε_{ij} the rate of dissipation, K_{ij} the direct effects of compressibility due to density fluctuations, $(\tilde{\ })$ Favre averaging, $(\bar{\ })$ nonweighted averaging, $(\ '')$ Favre fluctuations, and $(\ ')$ nonweighted fluctuations (for any flow quantity[20,21] b : $\tilde{b} + b'' = \bar{b} + b'$ and $\overline{b''} = \bar{b} - \tilde{b}$, and for any flow quantities[22] b_1 and b_2 : $\overline{b_1''b_2'} = \overline{b_1'b_2'} = \overline{b_1'b_2''}$), the transport equations for the Favre–Reynolds-averaged[20,21] Reynolds stresses are[22]

$$
\begin{aligned}
&\underbrace{\frac{\partial \bar{\rho}\widetilde{u_i''u_j''}}{\partial t} + \frac{\partial}{\partial x_l}\left(\bar{\rho}\widetilde{u_i''u_j''}\tilde{u}_l\right)}_{\text{convection } C_{ij}} \\
&\quad = \underbrace{\frac{\partial}{\partial x_l}\left(-\bar{\rho}\,\widetilde{u_i''u_j''u_l''} - \overline{p'u_j'}\delta_{il} - \overline{p'u_i'}\delta_{jl} + \overline{u_i'\tau_{jl}'} + \overline{u_j'\tau_{il}'}\right)}_{\text{diffusion } d_{ij} = -\partial T_{ijl}/\partial x_l} \\
&\qquad + \underbrace{\overline{p'\left(2D_{ij}' - \frac{2}{3}\frac{\partial u_k'}{\partial x_k}\delta_{ij}\right)}}_{\text{redistribution } \phi_{ij}} + \underbrace{\left(-\bar{\rho}\widetilde{u_i''u_l''}\frac{\partial \tilde{u}_j}{\partial x_l} - \bar{\rho}\widetilde{u_j''u_l''}\frac{\partial \tilde{u}_i}{\partial x_l}\right)}_{\text{production } P_{ij}} \\
&\qquad - \underbrace{\overline{\left(\tau_{jl}'\frac{\partial u_i'}{\partial x_l} + \tau_{il}'\frac{\partial u_j'}{\partial x_l}\right)}}_{\text{dissipation } \bar{\rho}\varepsilon_{ij}} + \underbrace{\frac{2}{3}\overline{p'\frac{\partial u_k'}{\partial x_k}}\delta_{ij}}_{\text{pressure-dilatation}} \\
&\qquad + \underbrace{\left(-\overline{u_i''}\frac{\partial \bar{p}}{\partial x_j} - \overline{u_j''}\frac{\partial \bar{p}}{\partial x_i} + \overline{u_i''}\frac{\partial \bar{\tau}_{jl}}{\partial x_l} + \overline{u_j''}\frac{\partial \bar{\tau}_{il}}{\partial x_l}\right)}_{\text{density fluctuation effects } K_{ij}}
\end{aligned}
\tag{1}
$$

Received Feb. 29, 1996; revision received April 10, 1996; accepted for publication Aug. 22, 1996; also published in *AIAA Journal on Disc*, Volume 2, Number 1.

*Professor, Director, Laboratoire d'Energétique, Unité Associée au Centre National de Recherche Scientifique 1504, Bâtiment 511.

†Assistant Professor, Laboratoire d'Energétique, Unité Associée au Centre National de Recherche Scientifique 1504, Bâtiment 511.

The compressible terms $\frac{2}{3}\overline{p'\Theta'}\delta_{ij}$ and K_{ij} are neglected, as is usual practice in transonic boundary-layer flow $\frac{2}{3}\overline{p'\Theta'}\delta_{ij} + K_{ij} \approx 0$. The other terms that require closure (C_{ij} and P_{ij} are exact terms) are modeled using a straightforward extension to compressible flow of the work of Launder and Shima,[9] based on replacing nonweighted averaging by Favre averaging. In this model, the near-wall effects are modeled making the model constants dependent on the local values of the invariants of the symmetric deviatoric anisotropy tensor[23] a_{ij}, A_1, A_2, and A_3:

$$a_{ij} = \frac{\widetilde{u_i''u_j''}}{k} - \frac{2}{3}\delta_{ij}; \qquad A_1 = a_{ii} = 0; \qquad A_2 = a_{ik}a_{ki}$$
$$A_3 = a_{ik}a_{kj}a_{ji}; \qquad A = \left[1 - \tfrac{9}{8}(A_2 - A_3)\right] \tag{2}$$

where $k = \frac{1}{2}\widetilde{u_i''u_i''}$ is the turbulence kinetic energy.

Diffusion due to turbulent transport is modeled by a simple Daly–Harlow model[24]

$$d_{ij} \approx \frac{\partial}{\partial x_l}\left\{\left[\mu(\tilde{T})\delta_{kl} + C_s\frac{k}{\varepsilon}\bar{\rho}\widetilde{u_k''u_l''}\right]\frac{\partial \widetilde{u_i''u_j''}}{\partial x_k}\right\}, \qquad C_s = 0.22 \tag{3}$$

where μ is the dynamic viscosity at Favre-averaged mean temperature $\tilde{T}$. This model can be improved using the model suggested by Fu,[25] which respects the symmetry of T_{ijk} (Eq. 1), but diffusion is negligible in the transport equation budget across a boundary layer.

Dissipation is modeled by a simple isotropic tensor $\bar{\rho}\varepsilon_{ij} \approx \frac{2}{3}\delta_{ij}\bar{\rho}\varepsilon$. Launder and Shima[9] note that, although this model is incorrect in the near-wall region,[26] the effects of ε_{ij} anisotropy are included in the model for ϕ_{ij1} and ϕ^w_{ij1}, by making the model coefficients functions of the anisotropy tensor invariants [Eq. (2)] and of the turbulence Reynolds number $Re_T = \bar{\rho}k^2\varepsilon^{-1}\mu^{-1}(\tilde{T})$.

The redistribution term ϕ_{ij} is split in slow and rapid parts[23] ϕ_{ij1} and ϕ_{ij2}, with wall-echo terms[27] ϕ^w_{ij1} and ϕ^w_{ij2}:

$$\phi_{ij} = \phi_{ij1} + \phi^w_{ij1} + \phi_{ij2} + \phi^w_{ij2} \tag{4}$$

$$\phi_{ij1} \approx -C_1\bar{\rho}\varepsilon a_{ij}, \quad C_1 = 1 + 2.58AA_2^{\frac{1}{4}}\{1 - \exp[-(0.0067Re_T)^2]\}$$
$$\phi_{ij2} \approx -C_2(P_{ij} - \tfrac{2}{3}\delta_{ij}P_k); \quad C_2 = 0.75\sqrt{A}$$
$$\phi^w_{ij1} \approx C^w_1(\varepsilon/k)\left[\bar{\rho}\widetilde{u_k''u_m''}n_kn_m\delta_{ij} - \tfrac{3}{2}\bar{\rho}\widetilde{u_k''u_i''}n_kn_j - \tfrac{3}{2}\bar{\rho}\widetilde{u_k''u_j''}n_kn_i\right]0.4(l_T/n) \tag{5}$$
$$C^w_1 = -\tfrac{2}{3}C_1 + 1.67$$
$$\phi^w_{ij2} \approx C^w_2\left[\phi_{km2}n_kn_m\delta_{ij} - \tfrac{3}{2}\phi_{ik2}n_kn_j - \tfrac{3}{2}\phi_{jk2}n_kn_i\right]0.4(l_T/n)$$
$$C^w_2 = \max\left[\left(\tfrac{2}{3}C_2 - \tfrac{1}{6}\right)/C_2, 0\right]$$

where n_i are the components of the unit normal on the wall, $P_k = \frac{1}{2}P_{ii}$ the turbulence kinetic energy production, and $l_T = k^{3/2}\varepsilon^{-1}$ the turbulence length scale. A detailed discussion of the coefficients of the ϕ_{ij} closure is given by Launder and Shima[9] and by Shima,[10,11] who discuss the connection between the form of C_1 and the realizability condition at the wall.[23]

One of the main difficulties in the implementation of the model is the choice of the normal to the wall, in the case of three-dimensional flow, in the corner region between two solid walls. The normal orientation and the distance from the wall appear in the models for ϕ^w_{ij1} and ϕ^w_{ij2}. In the case of a rectangular nozzle, there are four walls with normals $\mathbf{n}_A$, $\mathbf{n}_B$, $\mathbf{n}_C$, and $\mathbf{n}_D$, respectively. This problem was solved by computing separately the echo terms for each wall and then adding them together:

$$\phi^w_{ij} = \phi^{wA}_{ij} + \phi^{wB}_{ij} + \phi^{wC}_{ij} + \phi^{wD}_{ij} \tag{6}$$

Mean-Flow Energy Equation

It is common practice to use a modified pressure[28] $p* = \bar{p} + \frac{2}{3}\bar{\rho}k$ containing the turbulence kinetic energy $k = \frac{1}{2}\widetilde{u_i''u_i''}$ for Favre-averaged compressible flows. This is cumbersome when using Reynolds-stress closures, because the corresponding term ($\frac{2}{3}\bar{\rho}k$) must be substracted from the Reynolds stresses to avoid counting it twice. It was prefered to use an alternative, mathematically equivalent, treatment by adding a source term to the mean-flow energy equation. Defining $\breve{h}_t = \tilde{h} + \frac{1}{2}\tilde{u}_i\tilde{u}_i$ as the total enthalpy of the mean flow (which is different from the Favre-averaged total enthalpy $\tilde{h}_t = \tilde{h} + \frac{1}{2}\tilde{u}_i\tilde{u}_i + k = \breve{h}_t + k$), the exact mean-flow energy equation can be written[29]

$$\frac{\partial}{\partial t}(\bar{\rho}\breve{h}_t - \bar{p}) + \frac{\partial}{\partial x_l}(\bar{\rho}\tilde{u}_l\breve{h}_t) - \frac{\partial}{\partial x_l}\left[\tilde{u}_i(\bar{\tau}_{il} - \bar{\rho}\widetilde{u_i''u_l''}) - (\bar{\mathbf{q}}_l + \bar{\rho}\widetilde{e''u_l''})\right]$$
$$+ \underbrace{\frac{\partial\bar{\rho}k}{\partial t} + \frac{\partial}{\partial x_l}(\bar{\rho}\tilde{u}_lk) - \frac{\partial}{\partial x_l}\left(\overline{u_i'\tau_{il}'} - \overline{p'u_l'} - \frac{1}{2}\bar{\rho}\widetilde{u_i''u_i''u_l''}\right) - \overline{u_i''}\left(-\frac{\partial\bar{p}}{\partial x_i} + \frac{\partial\bar{\tau}_{il}}{\partial x_l}\right) - (-\bar{p}\delta_{il} + \bar{\tau}_{il})\frac{\partial\overline{u_i''}}{\partial x_l}}_{\frac{1}{2}C_{ii} - \frac{1}{2}d_{ii} - \frac{1}{2}K_{ii}} = 0 \tag{7}$$

where $\bar{\mathbf{q}}_l$ is the laminar heat-flux vector. Using the turbulence-kinetic-energy transport equation, which is one-half the trace of the Reynolds-stress transport equation (1),

$$\frac{1}{2}C_{ii} = \frac{1}{2}d_{ii} + \overbrace{\frac{1}{2}\phi_{ii}}^{\equiv 0} + \overbrace{\frac{1}{2}P_{ii}}^{\equiv P_k} - \overbrace{\frac{1}{2}\bar{\rho}\varepsilon_{ii}}^{\equiv\bar{\rho}\varepsilon} + \overline{p'\Theta'} + \frac{1}{2}K_{ii}$$
$$= \frac{1}{2}d_{ii} + P_k - \bar{\rho}\varepsilon + \overline{p'\Theta'} + \frac{1}{2}K_{ii} \tag{8}$$

the mean-flow energy equation can be written by replacing $\frac{1}{2}C_{ii} - \frac{1}{2}d_{ii} - \frac{1}{2}K_{ii} = P_k - \bar{\rho}\varepsilon + \overline{p'\Theta'}$ in Eq. (7):

$$\frac{\partial}{\partial t}(\bar{\rho}\breve{h}_t - \bar{p}) + \frac{\partial}{\partial x_l}(\bar{\rho}\tilde{u}_l\breve{h}_t)$$
$$- \frac{\partial}{\partial x_l}\left[\tilde{u}_i(\bar{\tau}_{il} - \bar{\rho}\widetilde{u_i''u_l''}) - (\bar{\mathbf{q}}_l + \bar{\rho}\widetilde{e''u_l''})\right]$$
$$= -\left[P_k - \bar{\rho}\varepsilon + \overline{p'\Theta'} - (-\bar{p}\delta_{il} + \bar{\tau}_{il})\frac{\partial\overline{u_i''}}{\partial x_l}\right] \tag{9}$$

This form of the transport equation for the mean-flow energy was used in this work. It makes clear the existence in the mean-flow energy equation of a sink term, equal to the net energy transferred to the fluctuating field ($P_k - \bar{\rho}\varepsilon$), including compressibility effects due to the pressure-dilatation correlation and to the work of the mean stresses (pressure + viscous) on the residual flow gradients due to density fluctuations ($\partial\overline{u_i''}/\partial x_l \equiv \partial(\bar{u}_i - \tilde{u}_i)/\partial x_l$). These compressible terms are neglected as was done for the Reynolds-stress transport equations, $\overline{p'\Theta'} - (-\bar{p}\delta_{il} + \bar{\tau}_{il})\partial\overline{u_i''}/\partial x_l \approx 0$.

Dissipation Equation

To avoid the instability associated with the wall boundary condition $\varepsilon_w = 2\breve{\nu}_w(\partial\sqrt{k}/\partial n)^2$, a compressible-flow extension to the Launder–Sharma[16] equation for the modified dissipation rate of the turbulence kinetic energy,

$$\varepsilon* = \varepsilon - 2\breve{\nu}(\text{grad}\sqrt{k})^2; \qquad \bar{\rho}\breve{\nu} = \mu(\tilde{T}) \tag{10}$$

for which the wall boundary condition is $\varepsilon^*_w = 0$, was used. The transport equation is the same as the one used in the Launder–Sharma k–$\varepsilon*$ turbulence closure[16] with the exception of the diffusion term, for which a tensorial diffusion coefficient is used, as is usual in Reynolds-stress closures.[4–12,27,30]

Flow Model Summary

The flow is modeled by the compressible Favre–Reynolds-averaged[20,21] three-dimensional Navier–Stokes equations, with Reynolds-stress transport closure, neglecting the compressible terms associated with density fluctuations:

$$\frac{\partial \bar{\rho}}{\partial t} + \frac{\partial \bar{\rho}\tilde{u}_l}{\partial x_l} = 0$$

$$\frac{\partial \bar{\rho}\tilde{u}_i}{\partial t} + \frac{\partial}{\partial x_l}[\bar{\rho}\tilde{u}_i\tilde{u}_l + \bar{p}\delta_{il}] - \frac{\partial(\bar{\tau}_{il} - \bar{\rho}\widetilde{u_i''u_l''})}{\partial x_l} = 0 \tag{11}$$

$$\frac{\partial(\bar{\rho}\breve{h}_t - \bar{p})}{\partial t} + \frac{\partial \bar{\rho}\tilde{u}_l\breve{h}_t}{\partial x_l} - \frac{\partial}{\partial x_l}[\tilde{u}_i(\bar{\tau}_{il} - \bar{\rho}\widetilde{u_i''u_l''})$$

$$-(\bar{\boldsymbol{q}}_l + \bar{\rho}\widetilde{e''u_l''})] + (P_k - \bar{\rho}\varepsilon) = 0 \tag{12}$$

$$\frac{\partial \bar{\rho}\widetilde{u_i''u_j''}}{\partial t} + \frac{\partial \bar{\rho}\tilde{u}_l\widetilde{u_i''u_j''}}{\partial x_l} - (d_{ij} + \phi_{ij} + P_{ij} - \bar{\rho}\varepsilon_{ij}) = 0 \tag{13}$$

$$\frac{\partial \bar{\rho}\varepsilon^*}{\partial t} + \frac{\partial}{\partial x_l}(\tilde{u}_l\bar{\rho}\varepsilon^*) - \frac{\partial}{\partial x_l}\left\{\left[\mu(\tilde{T})\delta_{kl} + C_\varepsilon\frac{k}{\varepsilon}\bar{\rho}\widetilde{u_k''u_l''}\right]\frac{\partial \varepsilon^*}{\partial x_k}\right\}$$

$$= C_{\varepsilon 1}P_k\frac{\varepsilon^*}{k} - C_{\varepsilon 2}\bar{\rho}\frac{\varepsilon^{*2}}{k} + E \tag{14}$$

$$\bar{p} = \bar{\rho}R_g\tilde{T} = \bar{\rho}\frac{\gamma - 1}{\gamma}\tilde{h} = \bar{\rho}(\gamma - 1)\tilde{e}$$

$$\bar{\tau}_{ij} = \mu(\tilde{T})\left(\frac{\partial \tilde{u}_i}{\partial x_j} + \frac{\partial \tilde{u}_j}{\partial x_i} - \frac{2}{3}\frac{\partial \tilde{u}_l}{\partial x_l}\delta_{ij}\right)$$

$$\bar{\boldsymbol{q}}_i = -\kappa(\tilde{T})\frac{\partial \tilde{T}}{\partial x_i}, \qquad \bar{\rho}\widetilde{e''u_i''} = -\kappa_T\frac{\partial \tilde{T}}{\partial x_i}$$

$$\mu(\tilde{T}) = \mu_{273}\frac{\tilde{T}^{\frac{3}{2}}}{273.15^{\frac{3}{2}}}\frac{110.4 + 273.15}{110.4 + \tilde{T}}$$

$$\kappa(\tilde{T}) = \kappa_{273}\frac{\mu(\tilde{T})}{\mu_{273}}[1 + 0.00023(\tilde{T} - 273.15)], \qquad \kappa_T = \frac{\mu_T c_p}{Pr_T}$$

$$Pr_T = 0.9, \qquad \mu_T = C_\mu\mu(\tilde{T})Re_T^*, \qquad c_p = \frac{\gamma - 1}{\gamma}R_g$$

$$Re_T^* = \frac{\bar{\rho}k^2}{\mu(\tilde{T})\varepsilon^*}, \qquad C_\varepsilon = 0.18, \qquad C_{\varepsilon 1} = 1.44 \tag{15}$$

$$C_{\varepsilon 2} = 1.92[1 - 0.3\exp(-Re_T^{*2})], \qquad E = \frac{2\mu(\tilde{T})\mu_T}{\bar{\rho}}(\nabla^2\tilde{\boldsymbol{V}})^2$$

$$C_\mu = 0.09\exp\left[-\frac{3.4}{(1 + 0.02Re_T^*)^2}\right], \qquad d_{ij}\text{: Eqs. (3)}$$

$$\phi_{ij}\text{: Eqs. (4), (5);} \qquad \bar{\rho}\varepsilon_{ij} = \tfrac{2}{3}\delta_{ij}\bar{\rho}\varepsilon$$

$$P_{ij} = \left(-\bar{\rho}\widetilde{u_i''u_l''}\frac{\partial \tilde{u}_j}{\partial x_l} - \bar{\rho}\widetilde{u_j''u_l''}\frac{\partial \tilde{u}_i}{\partial x_l}\right)$$

where $\gamma = 1.4$ is the isentropic exponent for air, $R_g = 287.04$ m^2 s^{-2} K^{-1} is the gas constant for air, μ_T is the eddy viscosity, κ_T is the eddy heat conductivity, $\mu_{273} = 17.11 \times 10^{-6}$ Pa s, and $\kappa_{273} = 0.0242$ W m^{-1} K^{-1}. The near-wall terms, accounting for the anisotropic part of the dissipation rate ($2\breve{\nu}[\text{grad}\sqrt{k}]^2$), and in the ε equation (E), are written in Cartesian tensor form, independently of the wall distance or orientation.[31,32]

Computational Method

Equations (11–14) are discretized in a structured grid using a finite volume technique, with vertex storage. The divergence of convective fluxes is discretized using the flux–vector-splitting method of Van Leer[33] with third-order MUSCL interpolation[34] and Van Albada limiters.[35] The velocity gradients and the divergence of viscous fluxes are computed using the second-order centered scheme described by Arnone,[36] and the control volume is computed as the sum of six pyramids.[37] This implementation follows closely the work of Anderson et al.,[38,39] and is a straightforward extension to Reynolds stress of the method used for the k–ϵ closure by Gerolymos and Vallet.[13] The discretization is described in detail by Vallet.[29]

The time discretization of the semidiscrete scheme uses a first-order implicit scheme. The resulting linear system is solved after approximate factorization of the Jacobian matrix of convective and viscous fluxes. Source terms are neglected in the implicit phase. Preliminary tests showed that their implicit treatment had no influence whatsoever on the stability of the method. The bandwidth of the spacewise systems is reduced using a spatially first-order-accurate approximation for the implicit term. Viscous terms are treated using a spectral radius approximation. The three successive spacewise linear systems are solved using banded-LU factorization.[40] The corresponding bandwidth is $(1 + 2 \times 23)$. Details are given by Vallet.[29]

The local time step is based on a combined convective (Courant) and viscous (von Neumann) criterion[41]:

$$\Delta t \leq \text{CFL}\min\left[\frac{l_g}{\tilde{V} + a\sqrt{1 + \frac{5}{6}(\gamma - 1)M_T^2}}, \frac{l_g^2}{2\nu_{\text{eq}}}\right]$$

$$\nu_{\text{eq}} = \frac{1}{\bar{\rho}}\max\left\{\frac{4}{3}[\mu(\tilde{T}) + \mu_T], \frac{\gamma - 1}{R_g}[\kappa(\tilde{T}) + \kappa_T]\right\} \tag{16}$$

where l_g is the grid cell size, $\tilde{V}$ the flow velocity, a the sound velocity, and ν_{eq} the equivalent diffusivity, computed by MacCormack.[42] Note that the turbulence Mach number[22] $M_T = \sqrt{(2ka^{-2})}$ appears in the convective stability time step, as has been demonstrated by many authors.[28,41] For steady computations, a Courant–Friedrichs–Lewy (CFL) $= 50$ is used with local time-stepping.

To achieve the high time steps used, it is indispensible to apply boundary conditions both implicitly and explicitly. At inflow, a reservoir condition is applied, whereas at the supersonic outflow all variables are extrapolated. A no-slip condition is applied on the adiabatic walls, where all turbulent quantities are set to zero. The inflow boundary condition is implemented using the theory of finite

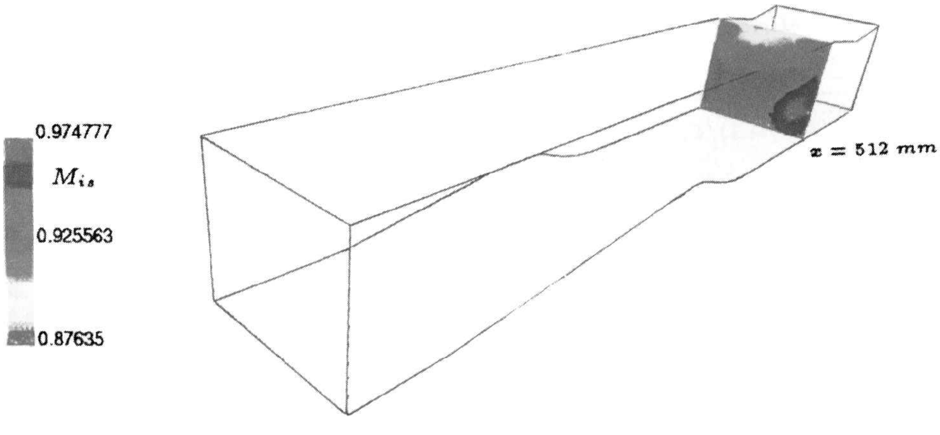

Fig. 1 Computed pressure inhomogeneity in a plane just before the throat for Delery three-dimensional configuration.

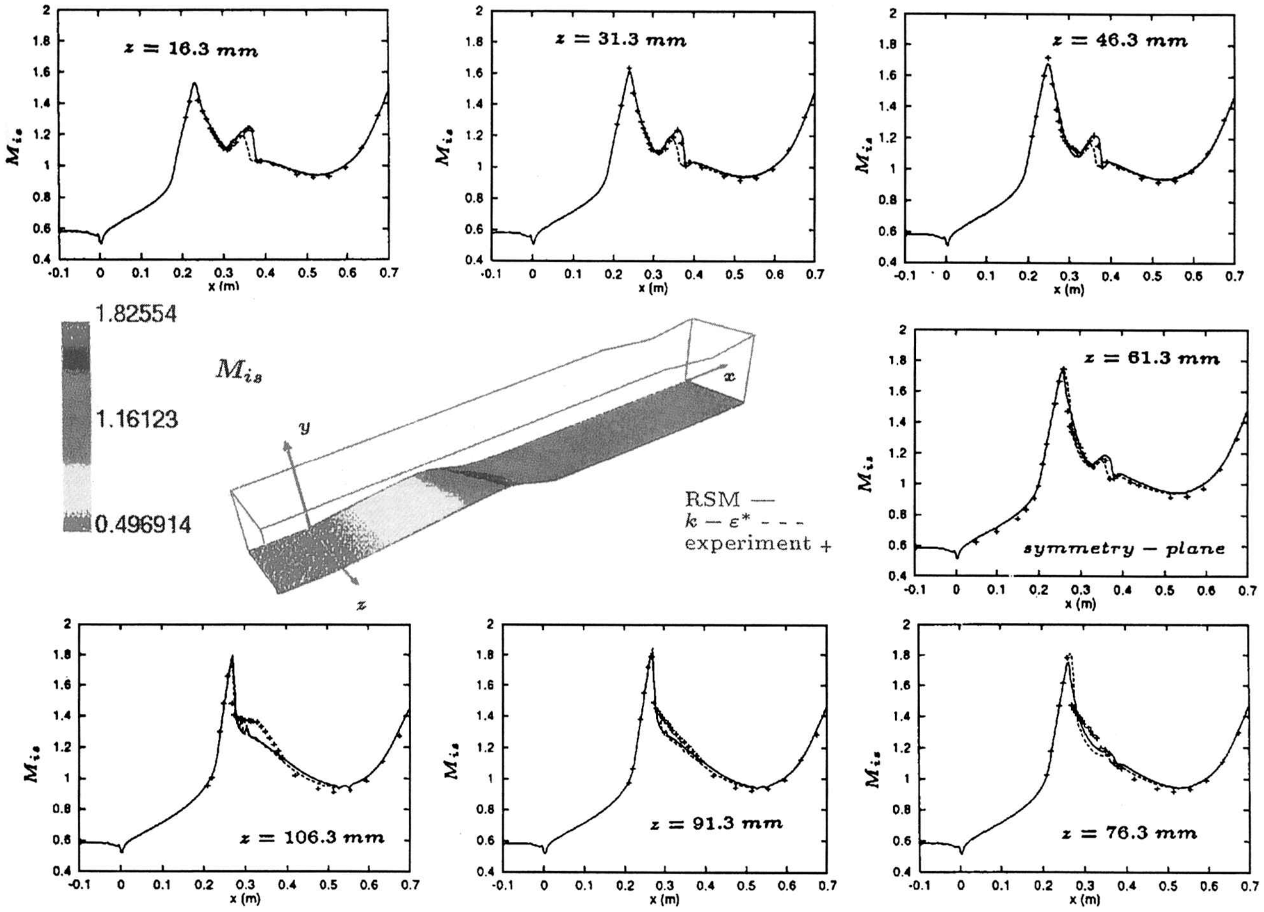

Fig. 2 Computed and measured M_{is_w} on the lower wall for Delery three-dimensional configuration.

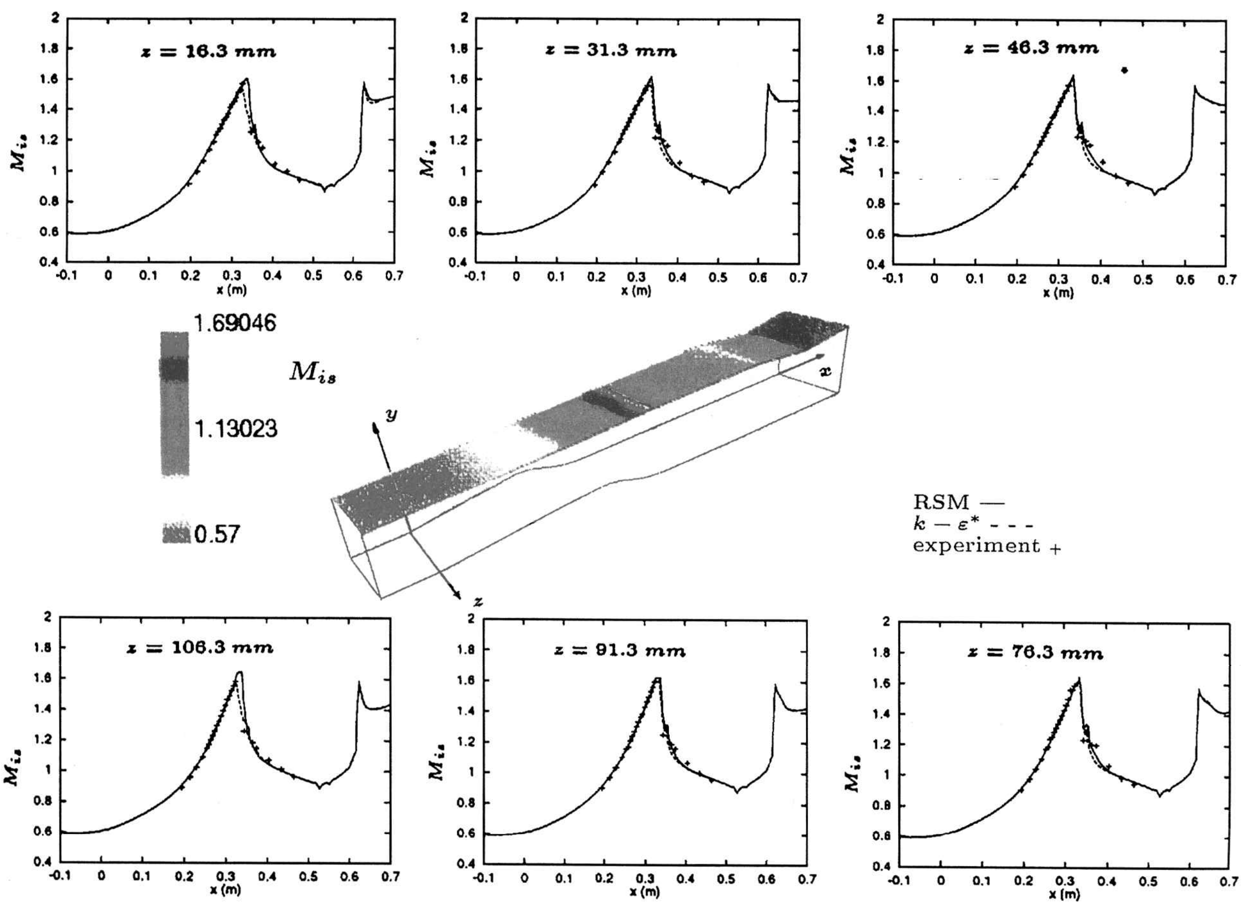

Fig. 3 Computed and measured M_{is_w} on the upper wall for Delery three-dimensional configuration.

waves,[43] and is treated implicitly following the corrections method of Chakravarthy,[44] to account for the outgoing pressure wave.

The initialization of the flowfield is a straightforward extension of the k–$\varepsilon*$ initialization used by Gerolymos and Vallet.[13] After obtaining the initial field for the mean flow, k, and $\varepsilon*$, the Reynolds-stress tensor is computed using a Boussinesq approximation for the shear stresses and the structure parameters measured by Laufer[45] in channel flow for the normal stresses. Details are given by Vallet.[29]

To ensure the stability of the method, it is necessary to introduce limiters for $\widetilde{\rho u_i'' u_j''}$ and $\varepsilon*$, which may otherwise diverge toward nonphysical values. The following very simple and particularly efficient limiters were used:

$$\text{if}\quad \left\{\widetilde{u''^2} < 0 \vee \widetilde{v''^2} < 0 \vee \widetilde{w''^2} < 0 \vee \varepsilon* < 0 \vee l_T^* = k^{\frac{3}{2}}\varepsilon*^{-1} > l_{T_{\max}}\right\}: \left\{\widetilde{u_i'' u_j''} \longleftarrow 0 \wedge \varepsilon* \longleftarrow 0\right\} \tag{17}$$

where $l_{T_{\max}}$ is a maximum admissible length scale (a characteristic order-of-magnitude length of the configuration). Divisions by zero are avoided throughout the code by adding 10^{-23} to the denominator [for every fraction $b_1/b_2 \approx b_1/(b_2 + 10^{-23})$]. Contrary to usual k–ε practice[13,32,46,47] no limiters were applied to turbulence production. This and our general experience with the model suggest that the present Reynolds-stress near-wall closure is more robust than classic k–ε closures.

Model Validation and Comparison with Delery Three-Dimensional Experiment

The Reynolds-stress model described above tends to the Launder–Reece–Rodi model[27] (LRR2 model) away from the walls (although with slightly modified coefficients, because C_1 and C_2 are always functions of the anisotropy). The modification to the Launder–Shima model[9] introduced in the present work concerns the near-wall terms of the ε equation. Validation is therefore necessary for wall-shear-layer flow. Computations were compared against the classic measurements of Klebanoff.[17] The agreement[29] is analogous with that

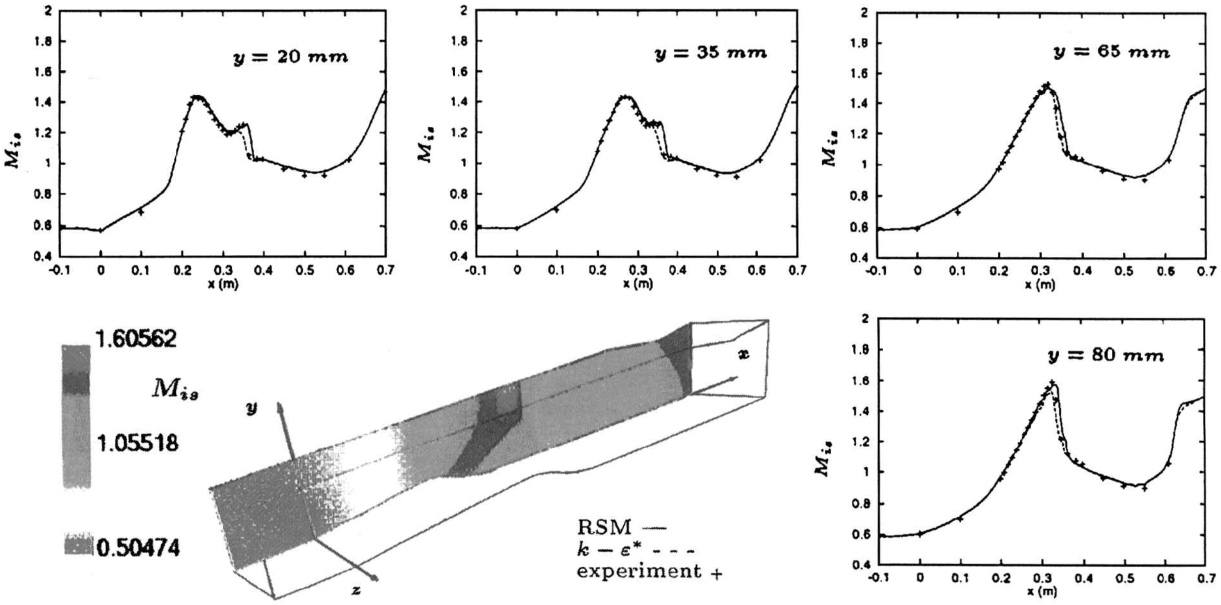

Fig. 4 Computed and measured M_{is_w} on the far wall for Delery three-dimensional configuration.

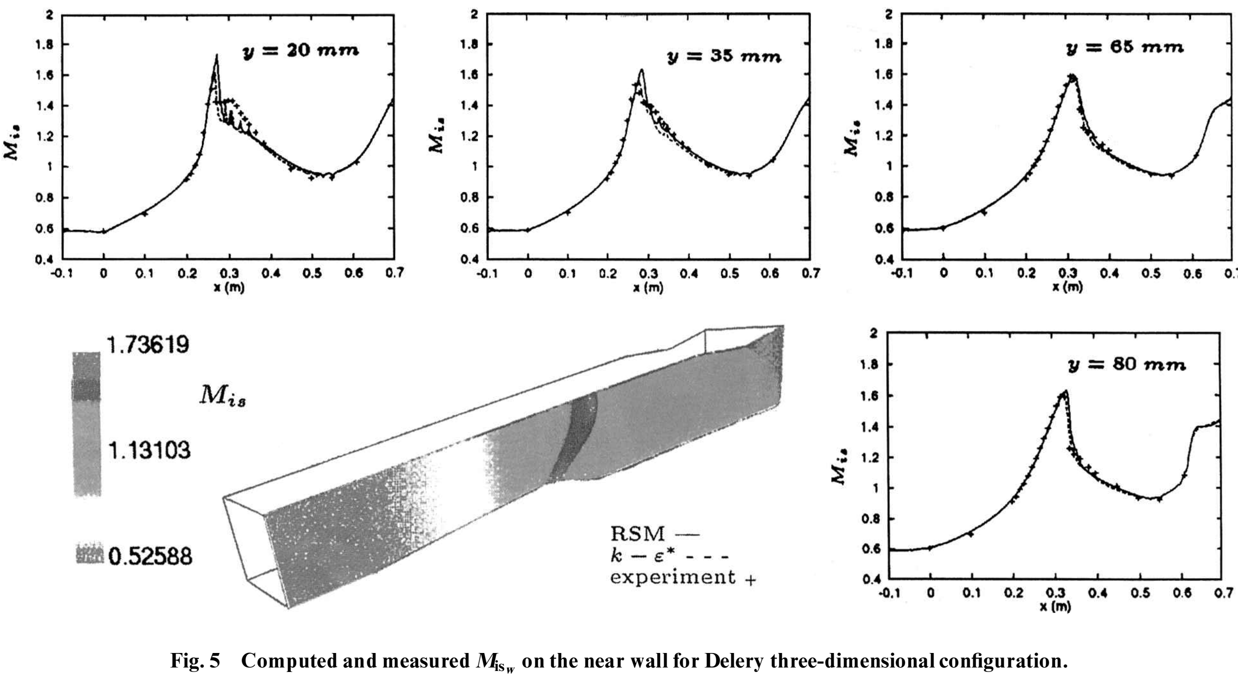

Fig. 5 Computed and measured M_{is_w} on the near wall for Delery three-dimensional configuration.

obtained by the original Launder–Shima model.[5,9] Detailed comparisons are given by Vallet.[29]

The Delery three-dimensional configuration (Table 1) is a rectangular nozzle. It has a swept three-dimensional bump on the lower wall. The upper wall is slightly sloped downward, and the two sidewalls are parallel planes. The experimental setup includes an adjustable 2. throat that is used to generate and adjust the shock wave.[18] This 2. throat is very near the trailing-edge bump (Fig. 1) so that the flow has not the leisure to homogenize. For this reason, computations that do not simulate the 2. throat are incorrect. In this work the 2. throat was discretized until a region of supersonic exit. Plotting the isentropic Mach number M_{is}:

$$M_{\text{is}}^2 = 2/(\gamma - 1)\left[(p_{t_1}/p)^{(\gamma-1)/\gamma} - 1\right]$$

in a crossflow plane in the region between the bump trailing-edge and the 2. throat illustrates the pressure inhomogeneity (53,000 $\pm$ 3000 Pa).

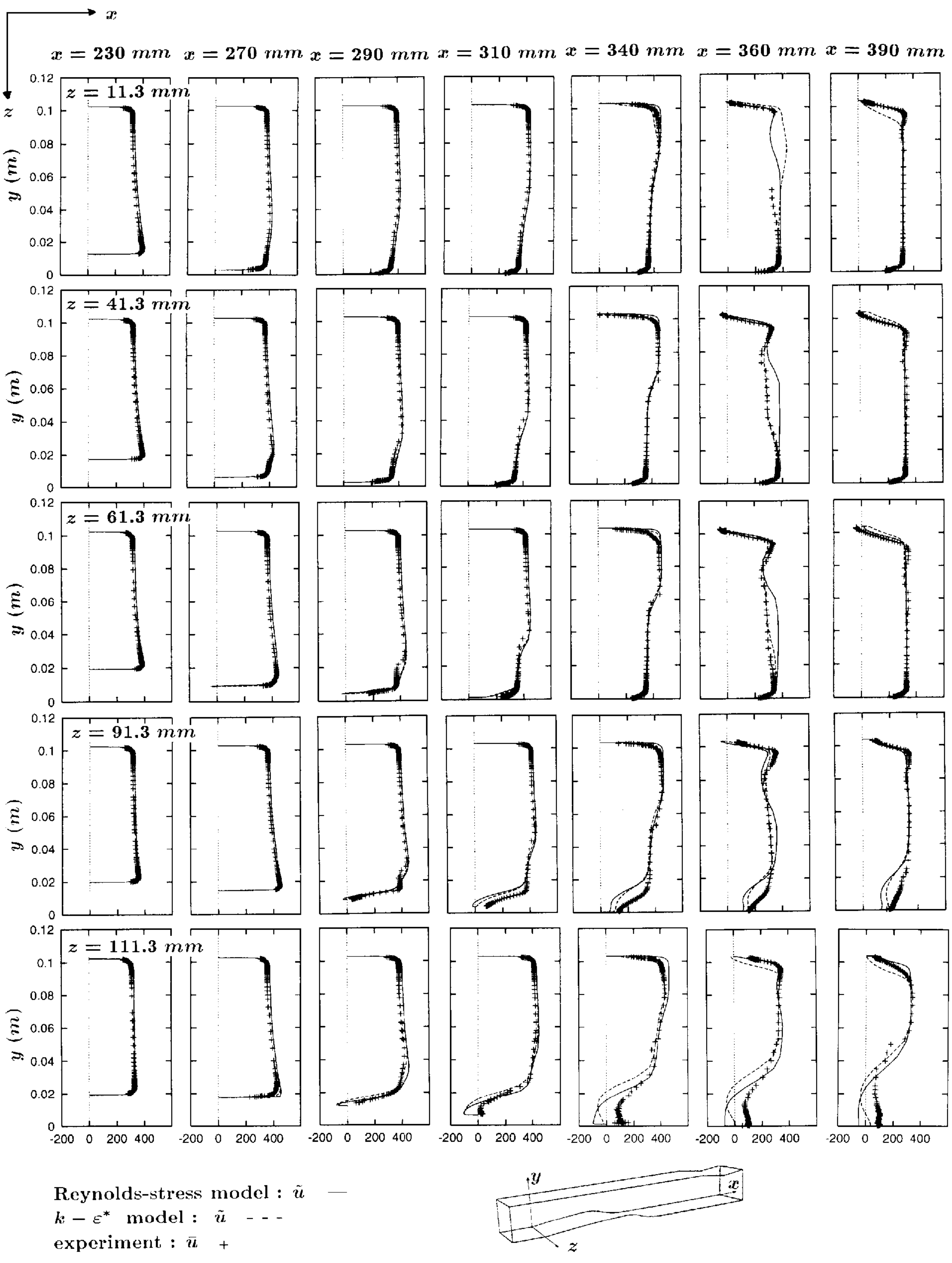

Fig. 6 Computed $\tilde{u}$ (m · s^{-1}) and measured $\bar{u}$ (m · s^{-1}) profiles for Delery three-dimensional configuration.

The experimental measurements[18,19] included wall-pressure taps, and laser Doppler velocimetry (LDV) of mean velocities and Reynolds stresses. The computations were performed on a $\sim$1.76 Mpoints grid (cf. Gerolymos and Vallet[13]), stretched geometrically near the walls, with $n_w^+ = 0.75$ everywhere (this has been verified by plotting n_w^+ of the converged flowfield).

Results using the Launder–Sharma[16] k–ε* model[13] also are presented. Comparison of computed and measured isentropic Mach number M_{is_w} on the lower wall (Fig. 2) show overall good agreement. The excellent prediction of the downstream reacceleration to supersonic flow, both for the k–ε* and the RSM computations, demonstrates the importance of simulating the 2. throat (the experimental throat height[48] was $\sim$95.6 mm and the simulated one 95 mm). The RSM computation is in excellent agreement with the measurements between the midspan plane ($z = 61.3$ mm) and the far wall ($z = 0$ mm), where the λ shock structure is accurately predicted,

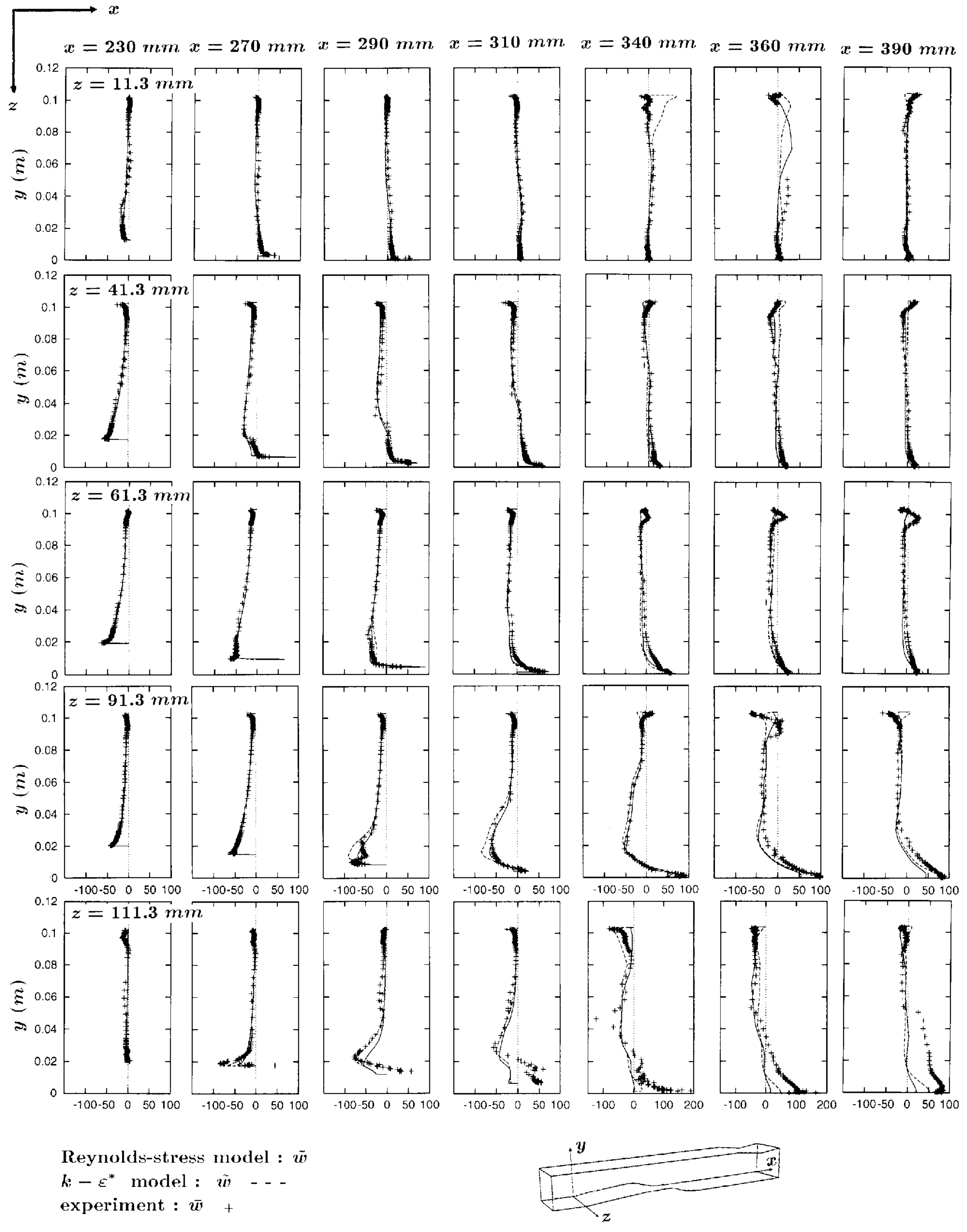

Fig. 7 Computed $\tilde{w}$(m s^{-1}) and measured $\bar{w}$(m s^{-1}) profiles for Delery three-dimensional configuration.

Table 1 Delery three-dimensional experiment[18,19]

$L_x \times L_y \times L_z$, mm	M_{shock}	Chord, χ	p_{t_1}	T_{t_1}	M_1	Re_χ
$800 \times 100 \times 121.3$	1.4–1.83	245–370 mm	0.092 MPa	300 K	0.57	$2.2–3.3 \times 10^6$

Table 2 Computing-time requirements for three-dimensional computations

Case	Model	Grid ($N_i \times N_j \times N_k$)	Mpoints[a]	Mwords	y_w^+	z_w^+	Iterations	CPU h[b]
Delery	k–$\varepsilon*$	$201 \times 91 \times 101$	1.76	141	0.75	0.75	900	31
three-dimensional	RSM	$201 \times 91 \times 101$	1.76	238	0.75	0.75	700	121

[a]1 Mpoint $= 1024^2$ points. [b]Cray C98.

whereas the k–$\varepsilon*$ model underpredicts the flow recceleration after the 1. shock wave, and as a consequence the 2. shock-wave strength. On the contrary, when approaching the near wall, both models fail to reproduce the pronounced pressure plateau observed experimentally.

On the upper wall (Fig. 3) the comparison of computed and measured results is quite satisfactory. There is no substantial detachment, and the pressure field shows negligible z-wise variation, in agreement with measurements.[18] Note that there is a confusion[48] of upper-wall and lower-wall experimental data in Cahen et al.[19] The 2. throat forms a sharp corner on the upper wall, the lower wall being flat. The expansion of the sonic flow at the sharp corner and the subsequent recompression are clearly seen on the M_{is_w} distributions on the upper wall (Fig. 3).

Comparison of computed and measured M_{is_w} distributions on the sidewalls (Figs. 4 and 5) corroborates the preceeding discussion, illustrating both the success of the RSM computations on the far wall and the inability of both models to predict the pronounced pressure plateau at the corner between the lower wall and the near wall (Fig. 5). Parasite spikes appearing in the M_{is_w} distributions are due to the Van Albada limiters.[35]

Detailed comparisons of computed $\tilde{u}$ and LDV-measured $\bar{u}$ profiles (Fig. 6) show that the RSM computations are in better agreement with measurements than the k–$\varepsilon*$ model, everywhere, except at the pressure-plateau region ($z = 91.3$ and 111.3). Examination of computed and measured velocities indicates that the computations predict a large streamwise detachment that was not observed in the experiment. The error is due to the strongly three-dimensional nature of the flow in this region, which appears when considering the spanwise velocities. Detailed comparisons of computed $\tilde{w}$ and LDV-measured $\bar{w}$ profiles (Fig. 7) show large discrepancies in the pressure-plateau region. The flow has a large spanwise velocity component, which convects air from the midspan region toward the near wall. This strong crossflow is then evacuated in the streamwise direction and is responsible for the absence of important streamwise detachment. Both models fail to predict this strongly three-dimensional flow. The inadequacy of the present RSM model was attributed to the very simple closure used for ϕ_{ij2} (Ref. 30), and eventually too-strong echo terms in the ϕ_{ij} closure.[49] The discrepancy also may be due partly to a lack of grid resolution, resulting in an unsatisfactory prediction of the secondary flows rather than a specific modeling of the pressure terms.

Computing-Time Requirements

The code runs on a Cray C98 computer. Its vectorization is adequate, but not outstanding ($\sim$200 Mflops), and computing-time requirements (Table 2) still can be substantially reduced. Note that a deliberate choice was made to minimize memory requirements, even at a small sacrifice of computational rapidity (the linear systems are solved on a plane-by-plane basis and not on a global one, thus diminishing vector performance).

Discussion and Conclusions

In this work, a near-wall RSM was developed, and numerically implemented. The model uses an $\varepsilon*$ equation that has the advantage of admitting the simple wall boundary condition $\varepsilon_w^* = 0$, and is therefore numerically very stable. The numerical method is a fully coupled implicit three-dimensional Navier–Stokes solver that is robust because of the use of efficient limiters for the turbulence quantities and admits CFL $= 50$ local time steps. The method was then applied to the computation of three-dimensional transonic flow in a rectangular nozzle. To the authors' knowledge, this is the first implementation of a near-wall RSM applied to three-dimensional transonic shock-wave/boundary-layer interaction.

Comparison with k–$\varepsilon*$ computations show that the RSM computations give overall better results, especially in the prediction of the λ shocks at the far wall. Both models fail to reproduce the three-dimensional structure of the large recirculating zone at the near wall. Note that the present RSM closure is more robust than the k–$\varepsilon*$ closure and requires less iterations to convergence.

The importance of simulating as closely as possible the experimental conditions, by simulating the adjustable 2. throat, has been shown. The authors believe that many computations of analogous configurations can be substantially improved in comparison with experiment, by including the computation of the 2. throat.

There are many possiblities for improving the turbulence model, in particular ϕ_{ij}, such as improving the ϕ_{ij2} closure, the wall-reflection terms, and the ε equation.

Acknowledgments

The computations presented in this work were run at the Institut pour le Dévelopement des Ressources en Informatique Scientifique, where computer resources were made available by the Comité Scientifique. The authors wish to thank J. M. Délery for providing the experimental data and discussing the results. Authors are listed alphabetically.

References

[1]Launder, B. E., "2-Moment Closure and Its Use in Modelling Turbulent Industrial Flows," *International Journal for Numerical Methods in Fluids*, Vol. 9, 1989, pp. 963–985.

[2]Leschziner, M. A., "Computation of Aerodynamic Flows with Turbulence-Transport Models Based on 2-Moment Closure," *Computers and Fluids*, Vol. 24, 1995, pp. 377–392.

[3]Launder, B. E., "Numerical Computation of Convective Heat Transfer in Complex Turbulent Flows: Time to Abandon Wall-Functions?" *International Journal of Heat and Mass Transfer*, Vol. 27, 1984, pp. 1485–1491.

[4]So, R. M. C., Lai, Y. G., and Hwang, B. C., "Near-Wall Turbulence Closure for Curved Flows," *AIAA Journal*, Vol. 29, No. 8, 1991, pp. 1202–1213.

[5]So, R. M. C., Lai, Y. G., Zhang, H. S., and Hwang, B. C., "2-Order Near-Wall Turbulence Closures: A Review," *AIAA Journal*, Vol. 29, No. 11, 1991, pp. 1819–1835.

[6]So, R. M. C., Zhang, H. S., and Speziale, C. G., "Near-Wall Modeling of the Dissipation-Rate Equation," *AIAA Journal*, Vol. 29, No. 12, 1991, pp. 2069–2076.

[7]Sotiropoulos, F., and Patel, V. C., "Prediction of Turbulent Flow Through a Transition Duct Using a Second-Moment Closure," *AIAA Journal*, Vol. 32, No. 11, 1994, pp. 2194–2204.

[8]Sotiropoulos, F., and Patel, V. C., "Application of Reynolds-Stress Transport Models to Stern and Wake Flows," *Journal of Ship Research*, Vol. 39, 1995, pp. 263–283.

[9]Launder, B. E., and Shima, N., "2-Moment Closure for the Near-Wall Sublayer: Development and Application," *AIAA Journal*, Vol. 27, No. 10, 1989, pp. 1319–1325.

[10]Shima, N., "Prediction of Turbulent Boundary-Layer Flows with a 2-Moment Closure: Part I—Effects of Periodic Pressure Gradient, Wall Transpiration, and Free-Stream Turbulence," *Journal of Fluids Engineering*, Vol. 115, 1993, pp. 56–63.

[11] Shima, N., "Prediction of Turbulent Boundary-Layer Flows with a 2-Moment Closure: Part II—Effects of Streamline Curvature and Spanwise Rotation," *Journal of Fluids Engineering*, Vol. 115, 1993, pp. 64–69.

[12] Ladeinde, F., "Supersonic Flux-Split Procedure for Second-Moments of Turbulence," *AIAA Journal*, Vol. 33, No. 7, 1995, pp. 1185–1195.

[13] Gerolymos, G. A., and Vallet, I., "Implicit Computation of Three-Dimensional Compressible Navier–Stokes Equations Using k–ϵ Closure," *AIAA Journal*, Vol. 34, No. 7, 1996, pp. 1321–1330.

[14] Jones, W. P., and Launder, B. E., "The Prediction of Laminarization with a 2-Equation Model of Turbulence," *International Journal of Heat and Mass Transfer*, Vol. 15, 1972, pp. 301–314.

[15] Jones, W. P., and Launder, B. E., "The Calculation of Low-Reynolds-Number Phenomena with a 2-Equation Model of Turbulence," *International Journal of Heat and Mass Transfer*, Vol. 16, 1973, pp. 1119–1130.

[16] Launder, B. E., and Sharma, B. I., "Application of the Energy Dissipation Model of Turbulence to the Calculation of Flows near a Spinning Disk," *Letters in Heat and Mass Transfer*, Vol. 1, 1974, pp. 131–138.

[17] Klebanoff, P. S., "Characteristics of Turbulence in a Boundary-Layer with Zero Pressure Gradient," NACA Rept. 1247, 1955.

[18] Benay, R., Délery, J. M., and Pot, T., "Analyse Expérimentale de l'Ecoulement dans un Canal Transsonique 3-D," *Recherche Aérospatiale*, Vol. 1986, No. 6, 1986, pp. 399–414.

[19] Cahen, J., Couailler, V., Délery, J., and Pot, T., "Validation of Code Using Turbulence Model Applied to Three-Dimensional Transonic Channel," *AIAA Journal*, Vol. 33, No. 4, 1995, pp. 671–679.

[20] Favre, A., "Equations des Gaz Turbulents Compressibles, Part 1: Formes Générales," *Journal de Mécanique*, Vol. 4, 1965, pp. 361–390.

[21] Favre, A., "Equations des Gaz Turbulents Compressibles, Part 2: Méthode des Vitesses Moyennes; Méthode des Vitesses Moyennes Pondérées par la Masse Volumique," *Journal de Mécanique*, Vol. 4, 1965, pp. 391–421.

[22] Sarkar, S., Erlebacher, G., Hussaini, M. Y., and Kreiss, H. O., "The Analysis and Modelling of Dilatational Terms in Compressible Turbulence," *Journal of Fluid Mechanics*, Vol. 227, 1991, pp. 473–493.

[23] Lumley, J. L., "Computational Modeling of Turbulent Flows," *Advances in Applied Mechanics*, Vol. 18, 1978, pp. 123–176.

[24] Daly, B. J., and Harlow, F. H., "Transport Equations in Turbulence," *Physics of Fluids*, Vol. 13, 1970, pp. 2634–2649.

[25] Fu, S., "Modelling of the Pressure-Velocity Correlation in Turbulence Diffusion," *Computers and Fluids Journal*, Vol. 22, 1993, pp. 199–205.

[26] Hanjalić, K., and Launder, B. E., "Contribution Towards a Reynolds-Stress Closure for Low-Reynolds-Number Turbulence," *Journal of Fluid Mechanics*, Vol. 74, 1976, pp. 593–610.

[27] Launder, B. E., Reece, G. J., and Rodi, W., "Progress in the Development of a Reynolds-Stress Turbulence Closure," *Journal of Fluid Mechanics*, Vol. 68, 1975, pp. 537–566.

[28] Vandromme, D., and Ha Minh, H., "About the Coupling of Turbulence Closure Models with Averaged Navier–Stokes Equations," *Journal of Computational Physics*, Vol. 65, 1986, pp. 386–409.

[29] Vallet, I., "Aérodynamique Numérique 3-D Instationnaire avec Fermeture Bas-Reynolds au Second Ordre," Ph.D. Dissertation, Dept. of Mechanics, Univ. Pierre-et-Marie-Curie, Paris, France, Dec. 1995.

[30] Launder, B. E., and Li, S. P., "On the Elimination of Wall-Topography Parameters from 2-Moment Closure," *Physics of Fluids*, Vol. 6, 1994, pp. 999–1006.

[31] Lakshminarayana, B., "Turbulence Modeling for Complex Shear Flows," *AIAA Journal*, Vol. 24, No. 12, 1986, pp. 1900–1917.

[32] Gerolymos, G. A., "Implicit Multiple-Grid Computation of the Compressible Navier–Stokes Equations Using k–ϵ Turbulence Closure," *AIAA Journal*, Vol. 28, No. 10, 1990, pp. 1707–1717.

[33] Van Leer, B., *Flux-Vector-Splitting for the Euler Equations*, Lecture Notes in Physics, Vol. 170, Springer–Verlag, 1982, pp. 507–512.

[34] Van Leer, B., "Towards the Ultimate Conservative Difference Scheme, Part V: A 2-Order Sequel to Godunov's Method," *Journal of Computational Physics*, Vol. 32, 1979, pp. 101–136.

[35] Van Albada, G. D., Van Leer, B., and Roberts, W. W., Jr., "A Comparative Study of Computational Methods in Cosmic Gas Dynamics," *Astronomy and Astrophysics*, Vol. 108, 1982, pp. 76–84.

[36] Arnone, A., "Viscous Analysis of 3-D Rotor Flow Using a Multigrid Method," *Journal of Turbomachinery*, Vol. 116, 1994, pp. 435–445.

[37] Vinokur, M., "An Analysis of Finite-Difference and Finite-Volume Formulations of Conservation Laws," *Journal of Computational Physics*, Vol. 81, 1989, pp. 1–52.

[38] Anderson, W. K., Thomas, J. L., and Van Leer, B., "Comparison of Finite-Volume Flux–Vector-Splittings for the Euler Equations," *AIAA Journal*, Vol. 24, No. 9, 1986, pp. 1453–1460.

[39] Anderson, W. K., Thomas, J. L., and Rumsey, C. L., "Extension and Application of Flux-Vector-Splitting to Calculations on Dynamic Meshes," *AIAA Journal*, Vol. 27, No. 6, 1989, pp. 673, 674; also AIAA Paper 87-1152, June 1987.

[40] Golub, G. H., and Van Loan, C. F., *Matrix Computations*, Johns Hopkins Univ. Press, Baltimore, MD, 1989, pp. 150–152.

[41] Kunz, R. F., and Lakshminarayana, B., "Stability of Explicit Navier–Stokes Procedures Using k–ϵ and k–ϵ/Algebraic Reynolds Stress Turbulence Models," *Journal of Computational Physics*, Vol. 103, 1992, pp. 141–159.

[42] MacCormack, R. W., "A Numerical Method for Solving the Equations of Compressible Viscous Flow," *AIAA Journal*, Vol. 20, No. 9, 1982, pp. 1275–1281.

[43] Atkins, H., and Casper, J., "Nonreflective Boundary Conditions for High-Order Methods," *AIAA Journal*, Vol. 32, No. 3, 1994, pp. 512–518.

[44] Chakravarthy, S. R., "Euler Equations—Implicit Schemes and Boundary Conditions," *AIAA Journal*, Vol. 21, No. 5, 1983, pp. 699–706.

[45] Laufer, J., "Investigation of Turbulent Flow in a 2-D Channel," NACA TN 2123, July 1950.

[46] Turner, M. G., and Jennions, I. K., "An Investigation of Turbulence Modeling in Transonic Fans Including a Novel Implementation of an Implicit k–ϵ Turbulence Model," *Journal of Turbomachinery*, Vol. 115, 1993, pp. 249–260.

[47] Jennions, I. K., and Turner, M. G., "3-D Navier–Stokes Computations of Transonic Fan Flow Using an Explicit Flow Solver and an Implicit k–ϵ Turbulence Model," *Journal of Turbomachinery*, Vol. 115, 1993, pp. 261–272.

[48] Délery, J. M., private communication, ONERA-Meudon, France, Aug. 1995.

[49] Launder, B. E., and Tselepidakis, D. P., "Directions in 2-Moment Modelling of Near-Wall Turbulence," AIAA Paper 91-0219, Jan. 1991.

Color reproduction courtesy of Laboratoire d'Energétique, Université Pierre-et-Marie-Curie